

See discussions, stats, and author profiles for this publication at: <https://www.researchgate.net/publication/263943621>

Antibacterial Efficiency of Graphene Nanosheets against Pathogenic Bacteria via Lipid Peroxidation

ARTICLE *in* THE JOURNAL OF PHYSICAL CHEMISTRY C · AUGUST 2012

Impact Factor: 4.77 · DOI: 10.1021/jp3047054

CITATIONS

59

READS

339

5 AUTHORS, INCLUDING:



Karthikeyan Krishnamoorthy

Jeju National University

66 PUBLICATIONS 1,174 CITATIONS

[SEE PROFILE](#)



Murugan Veerapandian

University of Guelph

48 PUBLICATIONS 625 CITATIONS

[SEE PROFILE](#)



Kyusik Yun

Gachon University

56 PUBLICATIONS 881 CITATIONS

[SEE PROFILE](#)

Antibacterial Efficiency of Graphene Nanosheets against Pathogenic Bacteria via Lipid Peroxidation

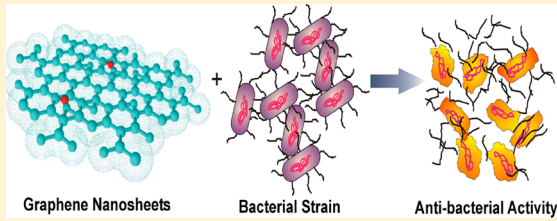
Karthikeyan Krishnamoorthy,[†] Murugan Veerapandian,[‡] Ling-He Zhang,[‡] Kyusik Yun,^{*,†,‡} and Sang Jae Kim^{*,†,§}

[†]Nanomaterials and System Lab, Department of Mechanical Engineering, Jeju National University, Jeju 690-456, Republic of Korea

[‡]Department of Bionanotechnology, Gachon University, Gyeonggi-do 461-701, Republic of Korea

[§]Department of Mechatronics Engineering, Jeju National University, Jeju 690-456, Republic of Korea

ABSTRACT: Graphene nanosheets are highly recognized for their utility toward the development of biomedical device applications. The present study investigated the antibacterial efficiency of graphene nanosheets against four types of pathogenic bacteria. Graphene nanosheets are synthesized by a hydrothermal approach (under alkaline conditions using hydrazine hydrate). UV-vis and X-ray diffraction show a maximum absorbance at 267 nm and appearance of new broad diffraction peak at 26°, which ensures the reduction of graphene oxide into graphene nanosheets. Stretching and bending vibrations of C–C bonds, chemical states, disorder, and defects associated with the graphene nanosheets are evaluated in comparison with graphene oxide. The minimum inhibitory concentration (MIC) of graphene nanosheets against pathogenic bacteria was evaluated by a microdilution method. MICs such as 1 $\mu\text{g}/\text{mL}$ (against *Escherichia coli* and *Salmonella typhimurium*), 8 $\mu\text{g}/\text{mL}$ (against *Enterococcus faecalis*), and 4 $\mu\text{g}/\text{mL}$ (against *Bacillus subtilis*) suggest that graphene nanosheets have predominant antibacterial activity compared to the standard antibiotic, kanamycin. Measurement of free radical modulation activity of graphene nanosheets suggested the involvement of reactive oxygen species in antibacterial properties.



INTRODUCTION

Graphene nanosheets have attracted a great deal of interest due to their fundamental importance and promising applications.¹ In fact, graphene as a two-dimensional material with high mobility and high carrier concentration has been extensively investigated for various fields and applications, such as field effect transistors, transparent conducting electrodes, supercapacitors, batteries, photocatalysis, gas sensors, field emission devices, and nanocomposites.^{2–4} Even though graphene is a promising candidate in electronic applications, research into the use of this material in biological applications is very limited and remains wide open. Recently, much interest is being drawn to the biological applications of graphene nanosheets. The preliminary research carried out shows that graphene could be an ideal candidate for biomedical applications such as photothermal therapy of cancer, gene transfection, and magnetic resonance imaging.^{5–7} Moreover, Hu et al. reported that graphene nanosheets are not toxic toward mammalian cells which is an added advantage for the use of graphene in bio-related applications.⁸ Graphene nanosheets due to their one atom thickness are an ideal candidate for the encasement of bacteria and other cellular components for transmission microscope imaging.⁹ It has been reported that graphene nanosheets are capable of acting as building block for bioelectronics at a molecular level.¹⁰ The application of graphene in the nanomedicine field is rapidly increasing and is an area of great interest.

Antibacterial agents are widely used in day-to-day life for the prevention of public health issues due to the ubiquitous of microorganisms and their ability to establish themselves.¹¹ In general, antibacterial agents are broadly categorized as organic or inorganic.¹² Organic antibacterial agents have disadvantages such as low heat resistance, high decomposability, and short life expectancy; these have limited their application and has resulted in the increasing use of inorganic antibacterial agents due to their improved safety and stability at higher temperatures.^{13,14} In this regard, the use of nanostructured materials with antibacterial properties is highly sought after owing to their ability to inhibit bacterial growth due to their size, structure, and surface properties.¹⁵ Several nanostructured materials with antibacterial properties, such as silver, copper, ZnO, MgO, TiO₂, CuO, carbon nanotubes (CNTs), and CNT-based materials, have received considerable attention in recent years.^{16–19} The use of nanomaterials with antibacterial properties is not only limited to *in vivo* applications, they can also be used for exterior applications such as paints, textiles, and in medical device applications so as to decrease the transfer of bacteria from any source to a healthy person.^{20,21} The multiple drug resistance of bacterial strains has led researchers to develop new antibacterial materials with low cost and effective antibacterial properties which could have significant impact on

Received: May 15, 2012

Revised: July 14, 2012

Published: July 18, 2012



the environment and health care.²² Graphene-based materials are also capable of acting as antibacterial agent due to their excellent physicochemical properties such as high thermal stability, high mechanical strength, biocompatibility, and often low cost.

Various efforts have been taken on the antibacterial activity of graphene based materials viz. Hu et al. investigated the activity of graphene-based antibacterial papers toward *E. coli* DH5α.⁸ Similarly, Okhavan et al. studied the toxicity of graphene and graphene oxide (GO) nanowalls toward *E. coli* and *S. aureus*.²² Lim et al. demonstrated the fabrication of graphene–chitosan composite films and investigated their antibacterial properties.²³ Krishnamoorthy et al. reported the antibacterial activity of GO-coated textile fabrics against *E. coli* and *S. aureus*.²⁴ Recently, graphene functionalized with antimicrobial peptides has been used for the bioselective detection of bacteria at cellular levels.²⁵ However, a detailed study on the antibacterial activity of graphene nanosheets with different bacterial strains and the mechanism of toxicity has not yet been reported until now. Examining antibacterial activity against different types of bacteria with an evaluation of minimum inhibition concentration (MIC) of graphene is an area of fundamental interest that needs to be investigated.

In this study, graphene nanosheets were prepared using a hydrothermal reduction of GO under alkaline conditions. The reduction of GO into graphene nanosheets was investigated by X-ray diffraction (XRD), UV-vis, Fourier-transform infrared (FTIR) spectra, X-ray photoelectron spectra (XPS), and Raman spectroscopic techniques. The antibacterial activity of the graphene nanosheets was studied against two Gram-negative and two Gram-positive bacterial strains by the microdilution method. The MIC values of the graphene nanosheets against both types of bacteria were measured and compared with a standard antibiotic drug, kanamycin.

■ EXPERIMENTAL SECTION

Materials and Methods. Graphite powder was purchased from Sigma-Aldrich Ltd. Potassium permanganate ($KMnO_4$), sulfuric acid (H_2SO_4), hydrogen peroxide (H_2O_2), hydrochloric acid (HCl), hydrazine hydrate, and sodium hydroxide (NaOH) were obtained from Dae Jung Chemicals and Metal Co., Ltd., South Korea. All the chemicals used in this research were research grade, and doubly distilled water is used throughout the experiments. The ultrasound irradiation was carried out on a SONIC VCX 750 model (20 kHz, 750 W) using a direct immersion titanium horn.

Synthesis of GO Nanosheets. The GO nanosheets were synthesized according to the modified Hummer's method using graphite powder as the starting material.²⁶ Briefly, graphite powder (2 g) was stirred in 98% H_2SO_4 (35 mL) for 1 h. Then, $KMnO_4$ (6 g) was gradually added to the above solution while keeping the temperature at less than 20 °C. The mixture was then stirred at 35 °C for 30 min. The resulting solution was diluted by adding 90 mL of water under vigorous stirring, and a dark brown color suspension was obtained. The reaction was terminated by the addition of 150 mL of distilled water and 30% H_2O_2 solution (5 mL). After being continuously stirred for 2 h, the mixture was washed by repeated centrifugation and filtration using a 5% HCl aqueous solution in order to remove any metal ions. Further, the centrifugation process was repeated with distilled water until the pH of the solution becomes neutral. The obtained brown precipitate is graphitic oxide and is dried under vacuum. Finally, 160 mL of water was added to the

resulting precipitate and sonicated well in a probe-type sonicator for nearly 1 h to obtain a uniform suspension of GO.

Hydrothermal Reduction of GO into Graphene Nanosheets. The reduction of GO into graphene nanosheets was achieved by the hydrothermal method. Briefly, 0.05 g of as-synthesized GO nanosheets was dispersed in 50 mL of deionized water and was irradiated by ultrasound for 30 min in order to achieve uniform dispersion of GO. Then the pH of the solution was adjusted to reach 10 by the addition of NaOH solution followed by the addition of 2 mL of hydrazine hydrate solution. Then, the solution is transferred into a Teflon vessel covered by a stainsteel reactor and kept at a constant temperature of 90 °C for 10 h. After the hydrothermal reaction, the obtained graphene nanosheets were washed thoroughly with distilled water and centrifuged at 12 000 rpm for 10 min in order to remove the residuals. The procedure was repeated several times until the synthesized product became free from trace amount of impurities. Further, the graphene nanosheets were dried in a hot air oven at 150 °C for 2 h in order to remove the water content.

Characterization Techniques. The crystal structure and orientation was determined by a Rigaku X-ray diffractometer (XRD) operated at 40 KeV and 40 mA with Cu K α radiation in the range of 10°–60° with a step of 0.02°. The UV-vis spectroscopy was performed using a Hewlett-Packard HP-8453 spectrophotometer. Scanning electron microscope measurement was performed on field emission scanning electron microscope (FE-SEM, JEOL JSM-7500F). Transmission electron microscope measurement was conducted on a TEM-JEOL instrument. The chemical composition and state of elements present in the outermost part of the GO and graphene nanosheets were obtained by X-ray photoelectron spectroscopy (XPS) techniques using ESCA-2000, VG Microtech Ltd. Here a monochromatic X-ray beam source at 1486.6 eV (aluminum anode) and 14 kV was used to scan the sample surface. A high-flux X-ray source with an aluminum anode was used for X-ray generation, and a quartz crystal monochromator was used to focus and scan the X-ray beam on the sample. Raman spectra of the GO and graphene nanosheets were produced using a LabRam HR800 micro-Raman spectroscope (Horiba Jobin-Yvon, France). The Raman system was operated at 10 mV laser power and an excitation wavelength of 514 nm with an Ar⁺ ion laser. The zeta potential measurements were carried out on a ZetaSizer (Nano-Z, Malvern Instruments Ltd. UK) using a laser Doppler microelectrophoresis technique with a 633 nm He–Ne laser as a light source.

Bacterial Strains. The as-synthesized graphene nanosheets were tested for antibacterial activity in comparison with a standard drug, kanamycin (aminoglycoside antibiotic). Four pathogenic bacterial strains including Gram-negative strains such as *Escherichia coli* (KACC 10005) and *Salmonella typhimurium* (KCCM 40253) and also Gram-positive strains such as *Bacillus subtilis* (KACC 14394) and *Enterococcus faecalis* (KACC 13807) were utilized in the study.

Test of Antibacterial Properties. The antibacterial activity of the samples was determined by the microdilution method.²⁷ LB broth was used as the diluent for the bacterial strains. Inoculates were prepared by suspending growth from overnight cultures in sterile LB media. The 2-fold dilution of samples and standard in the 96-well plates were prepared and denoted as graphene nanosheets and kanamycin. Approximately 10⁷ CFU/mL cells were inoculated; the final volume in each microwell plate was 0.2 mL and was incubated at 35 °C

for 24 h. The microwell plates were read at 590 nm using the ELISA reader before and after incubation to determine their MIC values. The MIC is defined as the lowest concentration of an antimicrobial agent that allows no growth of a microorganism after overnight incubation when compared with that of the control. The MIC of an antimicrobial drug corresponds to a lowered bacterial density from 10^7 to at least 10^2 CFU/mL (i.e., a 99.9% [$3 - \log_{10}$] reduction in bacterial inoculum).²⁸ The experiments were performed in triplicate and were repeated twice.

Lipid Peroxidation Measurement. The free radical modulation activity of graphene nanosheets was determined using a lipid peroxidation assay.¹⁷ Briefly, lipid peroxidation was induced in liposome prepared by ultrasonic irradiation from egg lecithin by adding 5 μ L of 400 mM FeCl₃ and 5 μ L of 200 mM L-ascorbic acid. To this, the graphene nanosheets were added. A control was prepared which contained no compound. The samples were incubated at 37 °C for 60 min. The reaction was inhibited by adding 1 mL of stopping solution which contained 0.25 N HCl, 1.5% trichloroacetic acid, and 0.375% thiobarbituric acid. These reaction mixtures were kept in a boiling water bath for 15 min, cooled, and centrifuged. The absorbance of the resulting solution was measured at 532 nm.

Statistical Analysis. Data were analyzed using Biostat software (AnalystSoft Inc., Vancouver, British Columbia, Canada) for one-way analysis of variance for the statistical significance of the model ($P < 0.05$).

RESULTS AND DISCUSSION

Synthesis of Graphene Nanosheets. Graphene nanosheets were successfully synthesized by improved hydrothermal reduction of GO. At first, the GO nanosheets are synthesized by the harsh oxidation of graphite followed by exfoliation as discussed in our previous report.²⁶ The obtained GO nanosheets are exfoliated into monolayers of GO by ultrasonication prior to the reduction reaction. The solution is adjusted to reach pH 10 by the addition of NaOH and then hydrazine hydrate followed by the hydrothermal treatment as described in the Experimental Section. The mechanism of reduction of GO into graphene nanosheets can be described as follows: GO with several oxygenated functional groups on its basal plane and at the edges can be deoxygenated in alkaline solution as suggested by Fan et al.²⁹ Hydrazine hydrate is commonly used for the reduction of functional groups in GO.³⁰ Additionally, the hydrothermal reaction enhances the reaction rate and kinetics due to the high pressure in hydrothermal conditions.³¹ The obtained graphene nanosheets are black in color, which confirms the reduction of GO into graphene nanosheets was successfully achieved.

UV-vis Spectroscopy Studies. A photographic image of the aqueous dispersions of graphene nanosheets (black) is shown in the inset of Figure 1. The change in color from brownish yellow (GO) to black confirms the reduction of GO into graphene by the hydrothermal approach.²⁹ The reduction of GO into graphene is characterized by UV-vis spectroscopy studies as shown in Figure 1. The UV-vis spectrum of GO shows a sharp absorption peak at 226 nm; this is attributed to the $\pi-\pi^*$ of the C-C aromatic rings.²⁶ After the reduction reaction, the absorption spectrum of graphene shows a maximum absorption at 267 nm.³² The occurrence of a redshift in the absorption spectra of graphene is due to the increased electron concentration due to removal of sp³ carbon

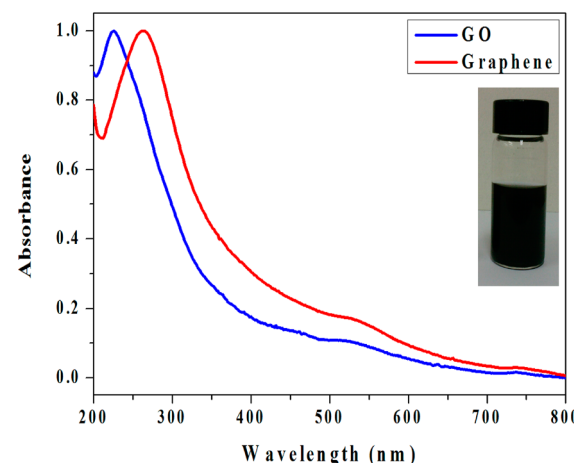


Figure 1. UV-vis spectra of GO and graphene nanosheets. Inset shows a photographic image of graphene dispersion.

atoms and is also consistent with the restoration of sp² carbon atoms.³³

X-ray Diffraction Studies. Figure 2 depicts the XRD pattern of the GO and graphene nanosheets. The diffraction

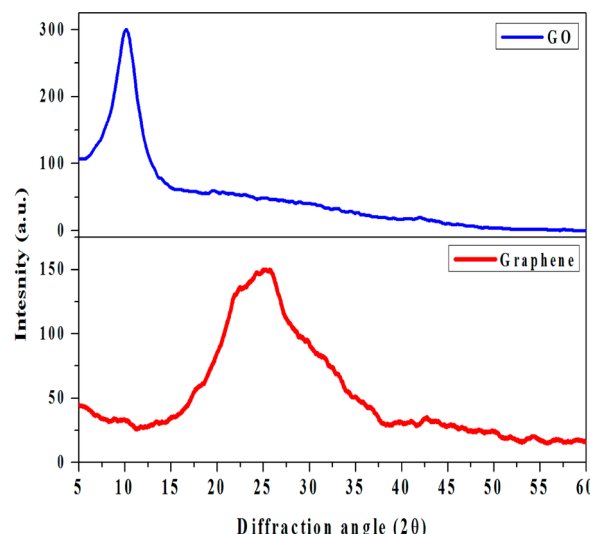


Figure 2. X-ray diffraction pattern of GO and graphene nanosheets.

peak of pure graphite is found around 26° as seen in our previous reports.³⁴ After successful oxidation, the diffraction peak of graphite at $2\theta = 26^\circ$ completely disappeared and a new broad peak around $2\theta = 10^\circ$ due to the oxidation of graphite appears. The corresponding interlayer spacing of GO was measured as 0.85 nm which is in agreement with results in previous published reports.²⁶ The reduction of GO into graphene is confirmed by the XRD pattern of graphene which shows a broad diffraction peak at $2\theta = 26^\circ$ corresponding to an interlayer spacing of 0.35 nm. The disappearance of the peak at $2\theta = 10^\circ$ in the GO and the formation of new broad peak at $2\theta = 26^\circ$ further supports that the GO is completely reduced into graphene. The obtained XRD results are in agreement with the previous findings of Zhang et al.³⁵

Surface Morphology Studies. Figure 3a,b shows the field-emission scanning electron micrograph (FE-SEM) of the hydrothermally synthesized graphene nanosheets with different magnifications. It shows the wavy features of graphene, which

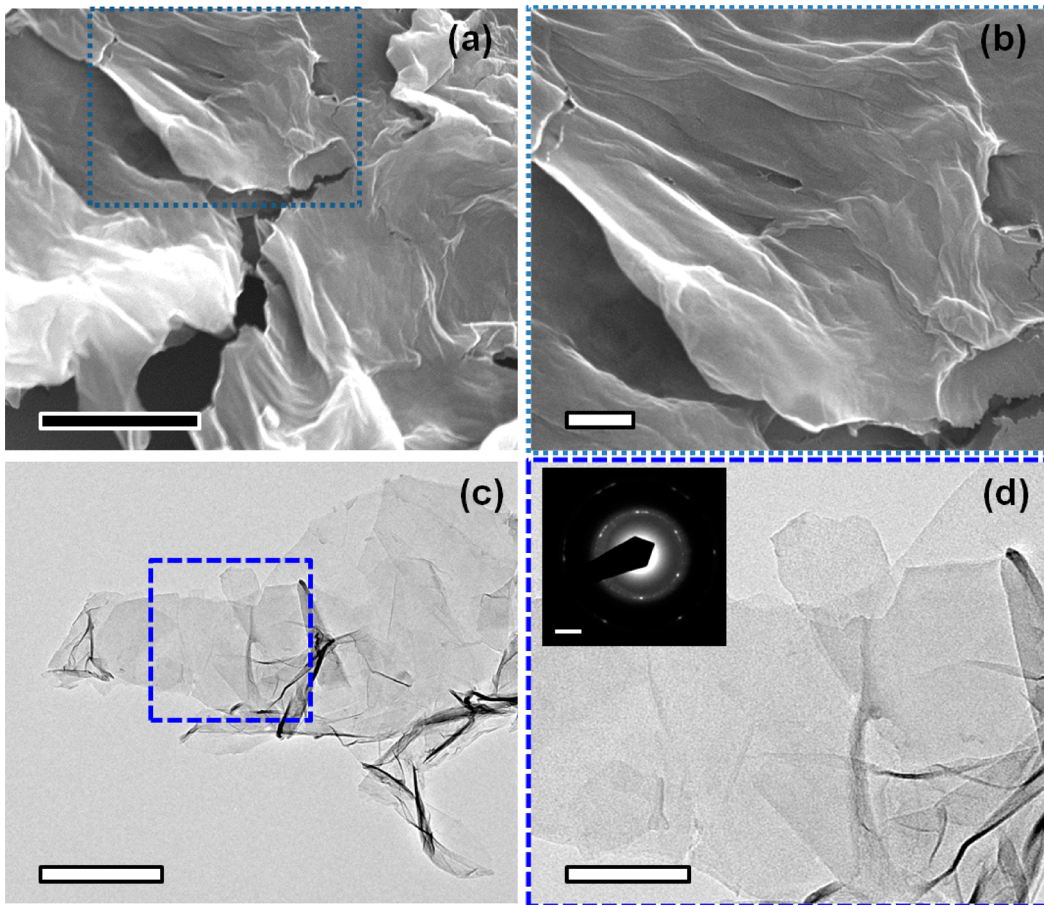


Figure 3. FE-SEM (a; scale bar = 1 μm ; b; scale bar = 100 nm) and HR-TEM images (c; scale bar = 200 nm; d; scale bar = 50 nm) of graphene nanosheets. Inset in (d) shows the SAED pattern of graphene nanosheets (scale bar = 2 nm^{-1}).

are due to the surface crumpling. Figure 3c,d shows the typical transmission electron microscopy images of the graphene nanosheets. It depicts that the sheets like morphology of graphene with high transparency. It also shows the presence of wrinkles and folded regions in the synthesized graphene nanosheets. The clear diffraction spots obtained in the SAED pattern (as shown in inset of Figure 3d) illustrate the hexagonal lattice and the discontinuity in the pattern is due to the superposition of two hexagonal patterns which is generally observed in few layer graphene.³⁶

FT-IR Studies. The FTIR spectra of GO and graphene nanosheets are measured to study the removal of oxygen containing functional groups in graphene after the reduction reaction. Figure 4 shows the FTIR spectra of the GO and graphene nanosheets. The FTIR spectra of the GO clearly show the presence of carboxyl, hydroxyl, epoxyl, and carbonyl groups at 1728, 1413, 1200, and 1050 cm^{-1} , respectively.³⁷ The peak due to the C–C vibrations from the graphitic domains is observed at 1600 cm^{-1} . In the FTIR spectra of graphene, the peak at 1600 cm^{-1} arises due to the C–C skeleton and the other peaks due to the oxygenated functional groups such as carboxyl, hydroxyl, epoxyl, and carbonyl groups are not observed, suggesting that GO was reduced into graphene nanosheets.³⁸

X-ray Photoelectron Studies. The chemical composition and state of elements present in GO and graphene are characterized by X-ray photoelectron spectroscopy. The comparative XPS spectra of GO and graphene nanosheets are

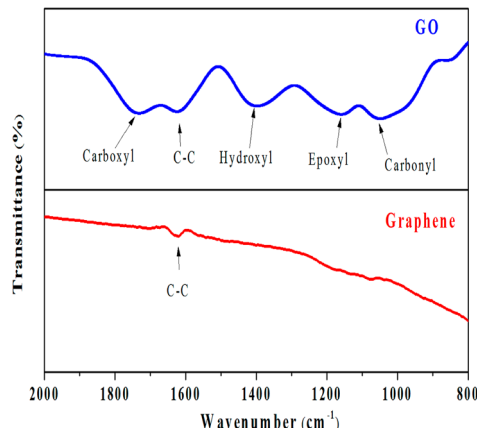


Figure 4. Fourier transform infrared spectra of GO and graphene nanosheets.

given in Figure 5. The XPS spectrum of the GO exhibited the characteristic peaks of C–C skeleton, hydroxyl, epoxyl, and carbonyl groups at 284.5, 286.2, 287.8, and 288.9 eV, respectively.³² The presence of these different oxygenated functional groups in GO is due to the oxidation of graphite which makes them hydrophilic in nature. The reduction of GO into graphene shows a drastic change in the XPS spectrum of graphene. From Figure 5, it is clear that graphene sheets show only the presence of a C–C skeleton (at 284.5 eV) with presence of a smaller amount of epoxyl groups. In comparison

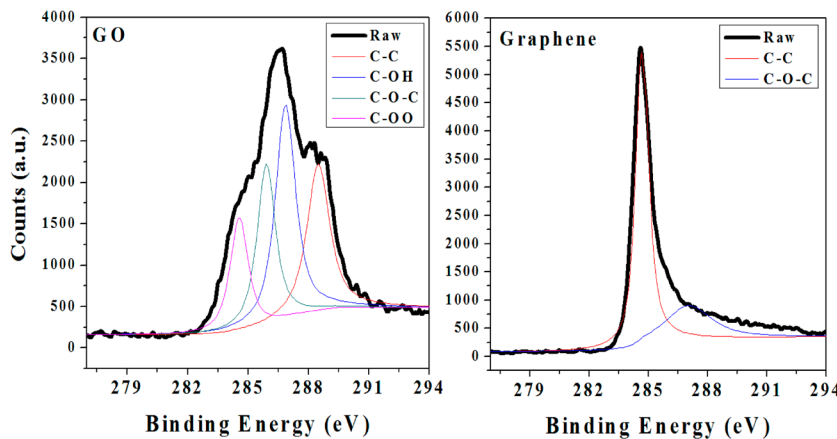


Figure 5. X-ray photoelectron spectra of GO and graphene nanosheets.

with the XPS of GO, the fact that the intensities of peaks related to the oxygen related functional groups such as hydroxyl, epoxyl, and carbonyl almost completely disappeared in the XPS of graphene further confirms the removal of the oxygenated functional groups due to the hydrothermal reduction process.³⁹

Raman Spectroscopic Investigations. Raman spectroscopy is a nondestructive technique to study the bonding nature of graphite materials such as CNT, GO, and graphene.⁴⁰ Raman spectroscopy was employed to study the crystallinity, disorder, and defect levels of the graphene nanosheets which are compared with GO. In general, the Raman spectrum of graphite exhibits a “G band” at 1570 cm^{-1} and a “D band” at 1350 cm^{-1} . The occurrence of the G band is due to the first-order scattering of the E_{2g} mode and the “D band” associates with the defects in the graphite lattice.⁴¹ The Raman spectrum of the GO and graphene nanosheets are shown in Figure 6. The

case of graphene, the G band is shifted toward a lower wavenumber (1589.41 cm^{-1}) due to the regraphitization that results in the formation of more sp^2 carbon atoms. This is in agreement with previous reports on chemically synthesized graphene.⁴² The D band becomes narrow and the intensity is increased, suggesting that the hydrothermal process modified the structure of graphene with defects.

The intensity of the G band ($I_{(G)}$) and D band ($I_{(D)}$) is used to measure the average crystallite size of the sp^2 domains. Cancodo et al. provided the general equation⁴³ of determination for the average crystallite size of the sp^2 domains L_a in the nanographite systems by relating the $I_{(D)}/I_{(G)}$ ratio to the fourth power of the laser energy used in the experiment as follows:

$$L_a \text{ (nm)} = [(2.4 \times 10^{-10})(\lambda_l)^4]/[I_{(D)}/I_{(G)}] \quad (1)$$

where L_a is the average crystallite size of the sp^2 domains, λ_l is the input laser energy, $I_{(D)}$ is the intensity of the D band, and $I_{(G)}$ is the intensity of the G band. The average crystallite sizes of the sp^2 domains in GO and graphene were measured as 15.45 and 11.76 nm, respectively. The average crystallite size of sp^2 domains is decreased in graphene compared to GO. This is due to the formation of new sp^2 carbon atoms which are smaller in size than the sp^2 carbon atoms present in GO before the reduction.³⁰ The decrease in FWHM of the G band in graphene ensures the formation of new sp^2 carbon atoms in graphene.

Zeta Potential Studies. The stability of nanomaterials in dispersion state is one significant issues for the biomedical applications of nanoparticles.⁴⁴ Hence, we measured the zeta potential of graphene nanosheets in an aqueous dispersion. The zeta potential of graphene nanosheets was found to be -26.75 mV (whereas the zeta potential of GO is -51.2 mV). It is well-known that GO has a highly negative zeta potential due to the ionization of edge carboxylic groups.⁴⁵ The reduction in zeta potential of the graphene nanosheets is attributed to the removal of functional groups after the reduction reaction. The observed zeta potential of graphene nanosheets (-26.75 mV) is well beyond the accepted values of colloidal stability ($\pm 25\text{ mV}$), indicating its high stability in dispersion.⁴⁶ The observed value of the zeta potential of graphene nanosheets is matched well with the previous published reports.⁴⁷

Antibacterial Activity of Graphene Nanosheets. In this study, the antibacterial activity of graphene nanosheets was tested using a microdilution method,²⁷ and the MIC values

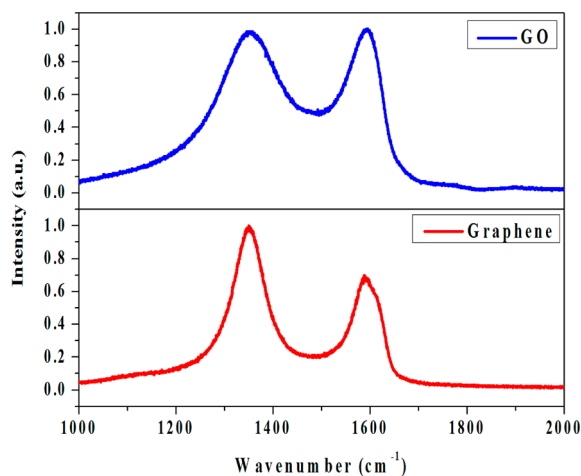


Figure 6. Raman spectra of GO and graphene nanosheets.

Raman spectrum of GO shows the presence of a G band at 1595.89 cm^{-1} and a D band at 1354 cm^{-1} . The G band in GO is shifted toward a higher wavenumber; this is due to the oxygenation of graphite which results in the formation of sp^3 carbon atoms. The D band in the GO is broadened due to the reduction in size of the in-plane sp^2 domains by the creation of defects, vacancies, and distortions of the sp^2 domains during oxidation.³⁰ The Raman spectrum of graphene shows significant changes compared with the spectrum of GO. In

were measured against two Gram-negative strains (*E. coli* and *S. typhimurium*) and Gram-positive strains (*E. faecalis* and *B. subtilis*). Antimicrobial properties of carbon-based materials such as CNT, fullerenes, graphite oxide, and in nanocomposite forms have been looked at in previous literatures.^{48–50} The general mechanism of antibacterial activity of carbon materials relies on the size, structure, composition, and properties of the individual materials. In addition, nanoscale size distribution, high surface to volume ratio, and other physicochemical properties were also demonstrated to be viable factors for governing antimicrobial effects.

Herein, a comparative analysis was performed to evaluate the antibacterial property of graphene nanosheets with a standard drug, kanamycin (aminoglycoside antibiotic). The MIC values of graphene nanosheets for both Gram-negative and Gram-positive bacteria are presented in Table 1. The MIC value of

Gram-positive bacteria. Our results showed that graphene nanosheets are more toxic to Gram-negative bacteria than Gram-positive bacteria. This is in agreement with previous findings of Hu et al. and Akhavan et al.^{8,22} Hu et al. reported that the antibacterial activity of graphene nanosheets results in the loss of cellular integrity with the disruption of cell walls of *E. coli*, which is due to either physical disruption or oxidative stress mechanism.⁸ In the present study, the differential toxicity of graphene toward Gram-negative bacteria compared to Gram-positive bacteria is due to differences in the natures of their cell walls. Gram-negative bacteria possess a thin peptidoglycan layer (7–8 nm thickness), whereas Gram-positive bacteria possess a thick peptidoglycan layer (about 20–80 nm thickness).^{22,51}

In general, the nanomaterials toxicity against biological systems arises due to physical disruption or oxidative stress.⁵² The former is due to direct contact between the nanomaterial and cellular systems while the latter is due to the generation of elevated ROS levels.⁵³ Understanding the nano-biointerface is a key aspect to elucidate the mechanism of cell death. Therefore, in the current study we observed the electron microscopic (FE-SEM) images of *E. coli* (as representative strain), before and after graphene exposure (see Figure 7). As seen in Figure 7c, the cell morphology of focused single *E. coli* cell clearly shows that the graphene sheets interaction with the bacterial surface causes the disruption of outer membrane, which leads to the cell death. This is in agreement with the previous study of Akhavan et al. in that they demonstrated the inactivation of bacteria by trapping the bacteria between the aggregated reduced graphene sheets by melatonin.⁵⁴ It should be also noted that nanomaterials toxicity toward biological species not only relies on the nature of the cell wall but also is dependent on cellular enzymes and biochemical events. There are reports showing that carbon-based materials such as CNT and fullerene cause oxidative stress in biological systems.^{48,49} The free-radical modulation activity of graphene nanosheets was determined by ultrasonic irradiation induced lipid peroxidation in liposomes from egg lecithin.¹⁷ Ultrasonic radiation caused lipid peroxidation in the liposomal membrane which results in the detection of three reaction products: conjugated dienes, lipid

Table 1. Minimum Inhibitory Concentration (MIC) of Graphene Nanosheets and Standard Drug Kanamycin^a against Gram-Negative and Gram-Positive Bacterial Strains^a

bacterial strains	graphene nanosheets MIC ($\mu\text{g/mL}$)	kanamycin MIC ($\mu\text{g/mL}$)
Gram-negative strains		
<i>Escherichia coli</i>	1	64
<i>Salmonella typhimurium</i>	1	64
Gram-positive strains		
<i>Enterococcus faecalis</i>	8	128
<i>Bacillus subtilis</i>	4	128

^aResults are mean \pm standard deviation ($n = 3$).

graphene against *E. coli*, *S. typhimurium*, *B. subtilis*, and *E. faecalis* were measured as 1, 1, 8, and 4 $\mu\text{g/mL}$, respectively. The MIC values of graphene nanosheets toward the tested bacterial species shows that it is more efficient compared with the MIC values of the standard antibiotic drug, kanamycin. Until now, there has been no such study measuring the MIC values of graphene nanosheets toward Gram-negative and

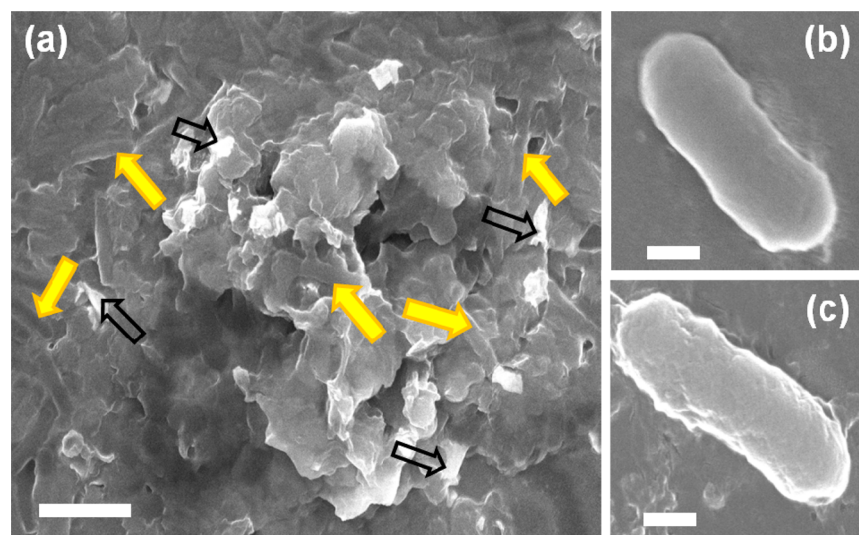


Figure 7. FE-SEM image of *E. coli* treated with graphene nanosheets (a: scale bar = 1 μm); focused single *E. coli* cell before (b: scale bar = 500 nm) and after antibacterial study (c: scale bar = 500 nm). Marked arrows shows in (a) denotes the location of graphene nanosheets (black arrow) and *E. coli* cells (yellow arrow) between the graphene nanosheets.

hydroperoxides, and malondialdehydes in the liposomal membrane.⁵⁵ These reaction products are produced at different stages of a lipid peroxidation chain reaction mediated by free radicals. Our earlier study demonstrates that lipid peroxidation is enhanced by ZnO nanoparticles.¹⁷ This evidence partly proves the involvement of free radicals in the reaction process.^{56,57}

Graphene nanosheets enhanced the ultrasound-induced lipid peroxidation. In comparison with the control group, lipid peroxidation was increased by 117% and 109% after exposure to 10 and 5 µg/mL of graphene ($p < 0.05$), respectively. This illustrates the influence of ROS in the toxicity of graphene nanosheets. Evidence for over production of reactive oxygen species (ROS) and its influence on the physiological effects in plants, bacteria, and mammalian cells by graphene was discussed in previous literatures.^{58,59} The mechanism of cellular toxicity such as elevated ROS levels that overwhelm the intracellular ROS levels causes cells to enter a state of oxidative stress which further results in damage to cellular components such as DNA, lipids, and proteins.^{39,60} The oxidation of fatty acids leads to the generation of lipid peroxides that stimulate a chain reaction, resulting in the disintegration of a cell membrane followed by cell death.¹⁷ Overall, our results on the antibacterial activity of graphene nanosheets show that graphene can act as a suitable antibacterial agent. Currently, we are focusing on the utilization of this material toward biomedical applications such as antibacterial textiles and coating of medical instruments for future work.

CONCLUSIONS

In conclusion, graphene nanosheets were synthesized by a hydrothermal method under alkaline conditions. The XRD and UV-vis spectra showed the formation of graphene nanosheets with a regraphitization process. The FE-SEM and HR-TEM studies showed the sheetlike morphology of the as-synthesized graphene. The FT-IR and XPS spectra confirmed the removal of oxygenated functional groups in graphene after the reduction reaction. The Raman spectroscopy illustrated the formation of new sp^2 carbon atoms in graphene due to the reduction of GO. Experimental results demonstrated that the prepared graphene nanosheets exhibit good antibacterial activity against the four tested bacterial species: *E.coli*, *S.typhimurium*, *B.subtilis*, and *E.faecalis*. The MIC values of graphene against these bacteria are very low compared with the MIC values of the standard antibiotic, suggesting that graphene can be effectively used as an antibacterial agent.

AUTHOR INFORMATION

Corresponding Author

*Tel: +82-64-754-3715; Fax: +82-64-756-3886; E-mail: kimsang@jejunu.ac.kr (S.J.K.). Fax: +82 31 7508819. E-mail: ykyusik@gachon.ac.kr (K.Y.).

Notes

The authors declare no competing financial interest.

ACKNOWLEDGMENTS

This research was supported by a National Research Foundation of Korea Grant under Contract 2011-0015829.

REFERENCES

- (1) Park, S.; Ruoff, R. S. *Nat. Nanotechnol.* **2009**, *4*, 217–224.
- (2) Lin, Z.; Liu, Y.; Yao, Y.; Hildreth, O. J.; Li, Z.; Moon, K.; Wong, C. *J. Phys. Chem. C* **2011**, *115*, 7120–7125.
- (3) Xu, C.; Wang, X.; Zhu, J. *J. Phys. Chem. C* **2008**, *112*, 19841–19845.
- (4) Schedin, F.; Geim, A. K.; Morozov, S. V.; Hill, E. W.; Blake, P.; Katsnelson, M. I.; Novoselov, K. S. *Nat. Mater.* **2007**, *6*, 652–655.
- (5) Yang, K.; Zhang, S.; Zhang, G.; Sun, X.; Lee, S. T.; Liu, Z. *Nano Lett.* **2010**, *10*, 3318–3323.
- (6) Feng, L.; Zhang, S.; Liu, Z. *Nanoscale* **2011**, *3*, 1252–1257.
- (7) Cong, H.-P.; He, J.-J.; Lu, Y.; Yu, S.-H. *Small* **2010**, *6*, 169–173.
- (8) Hu, W.; Peng, C.; Luo, W.; Lv, M.; Li, X.; Li, D.; Huang, Q.; Fan, C. *ACS Nano* **2010**, *4*, 4317–4323.
- (9) Mohanty, N.; Fahrenholz, M.; Nagaraja, A.; Boyle, D.; Berry, V. *Nano Lett.* **2011**, *11*, 1270–1275.
- (10) Mohanty, N.; Berry, V. *Nano Lett.* **2008**, *8*, 4469–4476.
- (11) Kim, J. S.; Kuk, E.; Yu, K. N.; Kim, J. H.; Park, S. J.; Lee, H. J.; Kim, S. H.; Park, Y. K.; Park, Y. H.; Hwang, C. Y.; Kim, Y. K.; Lee, Y. S. *Nanomedicine* **2007**, *3*, 95–101.
- (12) Sawai, J.; Yoshikawa, T. *J. Appl. Microbiol.* **2004**, *96*, 803–809.
- (13) Fang, M.; Chen, J. H.; Xu, X. L.; Yang, P. H.; Hildebrand, H. F. *Int. J. Antimicrob. Agents* **2006**, *27*, 513–517.
- (14) Jung, W. K.; Koo, H. C.; Kim, K. W.; Shin, S.; Kim, S. H.; Park, Y. H. *Appl. Environ. Microbiol.* **2008**, *74*, 2171–2178.
- (15) Raghupathi, K. R.; Koodali, R. T.; Manna, A. C. *Langmuir* **2011**, *27*, 4020–4028.
- (16) Veerapandian, M.; Lim, S. K.; Nam, H. M.; Kuppannan, G.; Yun, K. S. *Anal. Bioanal. Chem.* **2010**, *398*, 867–876.
- (17) Premanathan, M.; Karthikeyan, K.; Jayasubramanian, K.; Manivannan, G. *Nanomedicine* **2011**, *7*, 184–192.
- (18) Akhavan, O.; Azimirad, R.; Safad, S.; Hasani, E. *J. Mater. Chem.* **2011**, *21*, 9634–9640.
- (19) Kim, Y. H.; Lee, D. K.; Cha, H. G.; Kim, C. W.; Kang, Y. S. *J. Phys. Chem. C* **2007**, *111*, 3629–3635.
- (20) Veerapandian, M.; Yun, K. S. *Appl. Microbiol. Biotechnol.* **2011**, *90*, 1655–1667.
- (21) Kumar, A.; Vemula, P. K.; Ajayan, P. M.; John, G. *Nat. Mater.* **2008**, *7*, 236–241.
- (22) Akhavan, O.; Ghaderi, E. *ACS Nano* **2010**, *4*, 5731–5736.
- (23) Lim, H. N.; Huang, N. M.; Loo, C. H. *J. Non-Cryst. Solids* **2012**, *358*, 525–530.
- (24) Krishnamoorthy, K.; Navaneethaiyer, U.; Mohan, R.; Lee, J.; Kim, S.-J. *Appl. Nanosci.* **2012**, *2*, 119–126.
- (25) Mannoor, M. S.; Tao, H.; Clayton, J. D.; Sengupta, A.; Kaplan, D. L.; Naik, R. R.; Verma, N.; Omenetto, F. G.; McAlpine, M. C. *Nat. Commun.* **3**, Article number: 763 doi:10.1038/ncomms1767.
- (26) Krishnamoorthy, K.; Mohan, R.; Kim, S.-J. *Appl. Phys. Lett.* **2011**, *98*, 244101(1–3).
- (27) Amsterdam, D. In *Susceptibility Testing of Antimicrobials in Liquid Media*, 4th ed.; Lorian, V., Ed.; Lippincott Williams & Wilkins: Baltimore, MD, 1996; pp 52–111.
- (28) Levison, M. E. *Infect. Dis. Clin. North Am.* **2004**, *18*, 451–465.
- (29) Fan, X.; Peng, W.; Li, Y.; Li, X.; Wang, S.; Zhang, G.; Zhang, F. *Adv. Mater.* **2008**, *20*, 4490–4493.
- (30) Stankovich, S.; Dikin, D. A.; Piner, R. D.; Kohlhaas, K. A.; Kleinhammes, A.; Jia, Y.; Wu, Y.; Nguyen, S. T.; Ruoff, R. S. *Carbon* **2007**, *45*, 1558–1565.
- (31) Zhou, Y.; Bao, Q.; Tang, L. A. L.; Zhong, Y.; Loh, K. P. *Chem. Mater.* **2009**, *21*, 2950–2956.
- (32) Krishnamoorthy, K.; Veerapanidan, M.; Mohan, R.; Kim, S.-J. *Appl. Phys. A: Mater. Sci. Process.* **2012**, *106*, 501–507.
- (33) Chandra, S.; Sahu, S.; Pramanik, P. *Mater. Sci. Eng., B* **2010**, *167*, 133–136.
- (34) Venugopal, G.; Krishnamoorthy, K.; Mohan, R.; Kim, S.-J. *Mater. Chem. Phys.* **2012**, *132*, 29–33.
- (35) Zhang, J.; Yang, H.; Shen, G.; Cheng, P.; Zhang, J.; Guo, S. *Chem. Commun.* **2010**, *46*, 1112–1114.
- (36) Warner, J. H.; Rummeli, M. H.; Gemming, T.; Buchner, B.; Briggs, G. A. D. *Nano Lett.* **2009**, *9*, 102–106.
- (37) Si, Y.; Samulski, E. T. *Nano Lett.* **2008**, *8*, 1679–1682.

- (38) Zhu, C.; Guo, S.; Fang, Y.; Dong, S. *ACS Nano* **2010**, *4*, 2429–2437.
- (39) Gao, J.; Liu, F.; Liu, Y.; Ma, N.; Wang, Z.; Zhang, X. *Chem. Mater.* **2010**, *22*, 2213–2218.
- (40) Guo, H.-L.; Wang, X.-F.; Qian, Q.-Y.; Wang, F.-B.; Xia, X.-H. *ACS Nano* **2009**, *3*, 2653–2659.
- (41) Pimenta, M. A.; Dresselhaus, G.; Dresselhaus, M. S.; Cancado, L. G.; Jorio, A.; Saito, R. *Phys. Chem. Chem. Phys.* **2007**, *9*, 1276–1291.
- (42) Zhou, X.; Zhang, J.; Wu, H.; Yang, H.; Zhang, J.; Guo, S. *J. Phys. Chem. C* **2011**, *115*, 11957–11961.
- (43) Cancado, L. G.; Takai, K.; Enoki, T.; Endo, M.; Kim, Y. A.; Mizusaki, H.; Jorio, A.; Coelho, L. N.; Paniago, R. M.; Pimenta, M. A. *Appl. Phys. Lett.* **2006**, *88*, 163106(1–3).
- (44) Fang, C.; Bhattacharai, N.; Sun, C.; Zhang, M. *Small* **2009**, *5*, 1637–1641.
- (45) Yang, S.; Feng, X.; Ivanovici, S.; Mullen, K. *Angew. Chem., Int. Ed.* **2010**, *49*, 8408–8411.
- (46) Lotya, M.; Hernandez, Y.; King, P. J.; Smith, R. J.; Nicolosi, V.; Karlsson, L. S.; Blighe, F. M.; De, S.; Wang, Z.; McGovern, I. T.; Duesberg, G. S.; Coleman, J. N. *J. Am. Chem. Soc.* **2009**, *131*, 3611–3620.
- (47) Byon, H. R.; Lee, S. W.; Chen, S.; Hammond, P. T.; Horn, Y. S. *Carbon* **2011**, *49*, 457–467.
- (48) Zhang, Y.; Ali, S. F.; Dervishi, E.; Xu, Y.; Li, Z.; Casciano, D.; Biris, A. S. *ACS Nano* **2010**, *4*, 3181–3186.
- (49) Garza, K. M.; Soto, K. F.; Murr, L. E. *Int. J. Nanomed.* **2008**, *3*, 83–94.
- (50) Niu, A.; Han, Y.; Wu, J.; Yu, N.; Xu, Q. *J. Phys. Chem. C* **2010**, *114*, 12728–12735.
- (51) Eaton, P.; Fernandes, J. C.; Pereira, E.; Pintado, M. E.; Malcata, F. X. *Ultramicroscopy* **2008**, *108*, 1128–1134.
- (52) Lovric, J.; Cho, S. J.; Winnik, F. M.; Maysinger, D. *Chem. Biol.* **2005**, *12*, 1227–1234.
- (53) Xia, T.; Kovochich, M.; Brant, J.; Hotze, M.; Sempf, J.; Oberley, T.; Siloutas, C.; Yeh, J. I.; Weisner, M. R.; Nel, A. E. *Nano Lett.* **2006**, *6*, 1794–1807.
- (54) Akhavan, O.; Ghaderi, E.; Esfandiar, A. *J. Phys. Chem. B* **2011**, *115*, 6279–6288.
- (55) Jana, A. K.; Agarwal, S.; Chatterjee, S. N. *Radiat. Res.* **1990**, *124*, 7–14.
- (56) Pryor, W. A. The involvement of free radicals in aging and carcinogenesis. In Mathieu, V. J., Ed.; *Medicinal Chemistry*; Elsevier: Amsterdam, 1977; pp 331–59.
- (57) Pryor, W. A. Methods of detecting free radicals and free radical mediated pathology in environment toxicology. In Bhatnager, R. S., Ed.; *Molecular Basis of Environmental Toxicity*; Ann Arbor Publ. Inc.: Ann Arbor, MI, 1980; pp 3–36.
- (58) Li, Y.; Liu, Y.; Fu, Y.; Wei, T.; Guyader, L. L.; Gao, G.; Liu, R.-S.; Chang, Y.-Z.; Chen, C. *Biomaterials* **2012**, *33*, 402–411.
- (59) Liu, S.; Zeng, T. H.; Hofmann, M.; Burcombe, E.; Wei, J.; Jiang, R.; Kong, J.; Chen, Y. *ACS Nano* **2011**, *5*, 6971–6980.
- (60) Long, T. C.; Saleh, N.; Tilton, R. D.; Lowry, G. V.; Veronesi, B. *Environ. Sci. Technol.* **2006**, *40*, 4346–4352.